Journal of Materials Chemistry

Cite this: J. Mater. Chem., 2012, 22, 18181

www.rsc.org/materials

PAPER

Fascinating effect of dehydrogenation on the transport properties of *N*-heteropentacenes: transformation from p- to n-type semiconductor†

Xiao-Dan Tang,[ab] Yi Liao,*[ab] Hua Geng[c] and Zhi-Gang Shuai*[cd]

Received 14th May 2012, Accepted 12th July 2012
DOI: 10.1039/c2jm33039c

The fascinating effect of dehydrogenation on the charge transport properties of *N*-heteropentacene (**N-PEN**) derivatives was systematically investigated through Marcus electron transfer theory coupled with normal mode analysis distributed into internal coordinates for the reorganization energies and the random walk simulation of charge diffusion constants. The calculated results show that dehydrogenation of **N-PEN** derivatives will markedly increase the electron transfer integrals and simultaneously decrease the energy levels of the lowest unoccupied molecular orbitals (LUMOs) as well as the electron reorganization energies (λ_e), which provides a three-in-one advantage for improving the electron transfer. The lower LUMO levels detected in the dehydrogenated **N-PENs** compared to the hydrogenated ones can be inferred from their electronic structures, that is, the latter are formally antiaromatic, having 2 more electrons than the former (aromatic 22 π electron species). The reduced reorganization energies of the dehydrogenated **N-PENs** could be intimately connected to the bonding nature of the nitrogen atoms in the LUMOs. Upon the dehydrogenation of **N-PENs**, the effective intermolecular π-overlap in the LUMOs of the nearest-neighboring molecules is enhanced, and then increased the electron transfer integrals. Interestingly, the transport parameters evaluated from the band and hopping models both indicate intrinsic mobility for electron transfer in the dehydrogenated **N-PENs**. The dehydrogenation of **N-PEN** derivatives can, thus, be a useful strategy for preparing n-type organic semiconductors.

Introduction

Organic semiconductors (OSC) are of great interest because of their potential applications in electronic devices, including organic field-effect transistors (OFETs),[1–4] light-emitting diodes,[5,6] and photovoltaics.[7–9] In the past decade, most investigations in this field have been devoted to p-type OSCs.[10–15] However, the development of n-type OSCs is hindered because of the high injection barrier of electrons and the instability of radical anions in the air.

The potential of nitrogen-rich heteroacenes as n-type semiconductors has been recently proposed both experimentally[16–19] and theoretically.[20–24] Chao[20] and Winkler[21] groups predicted from their B3LYP calculations that the integration of more nitrogen atoms into the pentacene (**PEN**) scaffold (at least 5) may improve the electron affinity (EA) and facilitate electron transfer. Miao's group demonstrated that silylethynyl substituted *N*-heteropentacenes, **TIPS-TAP-2*p***, (Fig. 1), rank among the best performing n-type semiconductors with field-effect mobilities up to 3.3 $cm^2 V^{-1} s^{-1}$ under vacuum.[18] Three factors, the high EA, small electron reorganization energies (λ_e), and large electronic coupling originating from dense π-stacking are considered to result in the excellent electron transport of **TIPS-TAP-2*p***.[22,24] It has long been recognized that strategies for molecular design to improve EA, such as lateral substitution with electron-withdrawing groups,

[a]*Department of Chemistry, Capital Normal University, Beijing 100048, People's Republic of China. E-mail: yliao@cnu.edu.cn*
[b]*Institute of Functional Material Chemistry, Faculty of Chemistry, Northeast Normal University, Changchun 130024, Jilin, People's Republic of China*
[c]*Key Laboratory of Organic Solids, Beijing National Laboratory for Molecular Science (BNLMS), Institute of Chemistry, Chinese Academy of Sciences, 100190 Beijing, P R China. E-mail: zgshuai@tsinghua.edu.cn*
[d]*Key Laboratory of Organic OptoElectronics and Molecular Engineering, Department of Chemistry, Tsinghua University, 100084 Beijing, P R China*

† Electronic supplementary information (ESI) available: The reorganization energies of **TIPS-DHDAP-2*p***, **TIPS-DHTAP-2*p***, **TIPS-DAP-2*p*** and **TIPS-TAP-2*p*** calculated with B3LYP/6-31G* and 6-31 + G**, relative AIP, AEA, HOMO and LUMO energy levels of all systems calculated at B3LYP/6-31G* level, the percentage composition of the LUMO and HOMO for all systems in terms of **segments 1–3**, the evolution trends in λ_h and λ_e obtained with BLYP, B3LYP, PBE0 and BHHLYP methods and 6-31G* basis set, the molecular packings and dimer type pathways (D1 and D2) of systems **TIPS-DAP-1*p*** and **TIPS-DAP-1*t***, the relative energy curves of **DHTAP-2*p*** (blue) and **TIPS-DHTAP-2*p*** (black) from 1D-parallel to 2D-brick arrangement with ωB97XD (solid line), B97D (dashed line) and B3LYP-D (dotted line) functionals at 3-21G* level, and NBO analysis of C–H···π interactions in **TIPS-DHTAP-2*p*** with 1D-parallel arrangement. See DOI: 10.1039/c2jm33039c

often incur an adverse increase in the reorganization energy. In order to compare the performance of core substitution with imine nitrogen to lateral substitution with electron-deficient groups which are commonly used in the functionalization of n-type semiconductors, we roughly estimated the λ_e of three **PEN** derivatives, **N4-PEN**, **O4-PEN**, and **F12-PEN**. The number of heteroatoms is selected based on the precondition that these **PEN** derivatives have comparable EA values to those of the typical n-type materials, naphthalene and perylenetetracarboxylic diimides (**NDI** and **PDI**) (Scheme 1). The smallest λ_e of 171.3 meV was predicted at B3LYP/6-31G* level for **N4-PEN**, which exhibits optimal tradeoff between EA and λ_e.

The appealing features of *N*-heteropentacenes (**N-PENs**) for electron transport have stimulated great interest in the research of novel synthetic routes[25–33] and in the study of the structure–property relationships at the molecular level.[22,34–39] An issue which has long been underappreciated in this field is the hydrogenation (reduction) of **N-PENs** to their formally antiaromatic congeners. Diazapentacene (**DAP**) and dihydrodiazapentacene (**DHDAP**) are a redox interconvertible pair of **N-PENs**, of which the aromaticity and stability were recently explored by Wu *et al.*[40] Reduced $4n\pi$ **DHDAP** and the oxidized $4n + 2\pi$ **DAP** counterpart are stable in air. Studies of silylethynyl substituted *N*-heteroacenes[18,19] have also found that both **TIPS-DHDAP** and **TIPS-DAP** are stable in air and the former can be converted to the latter by oxidization with MnO_2. An interesting phenomenon concerning these stable redox pairs noticed by us is that the dehydrogenated forms always have better electron transfer potential than the corresponding hydrogenated ones. For example, the chlorinated dihydrodiazapentacene (**TCDAHP**) acted as a p-type semiconductor when its film was deposited on a **PEN** buffer layer, exhibiting a hole mobility of up to 1.4 $cm^2\ V^{-1}\ s^{-1}$.[41] In contrast, the dehydrogenated **TCDAP** behaved as an n-type semiconductor in OFETs with a very high electron mobility in the range of 2.50 to 3.39 $cm^2\ V^{-1}\ s^{-1}$.[42] In a similar way, the electron transport of the dehydrogenated **TIPS-TAP-2*p*** and **TIPS-DAP-2*p***, are also superior to those of the corresponding hydrogenated **TIPS-DHTAP-2*p*** and **TIPS-DHDAP-2*p*** (shown in Fig. 1), respectively.[18] It is quite natural to question why the simple hydrogen atom has such a wonderful influence on the transport properties when it is attached to or deleted from nitrogen atoms embedded in the **PEN** scaffold.

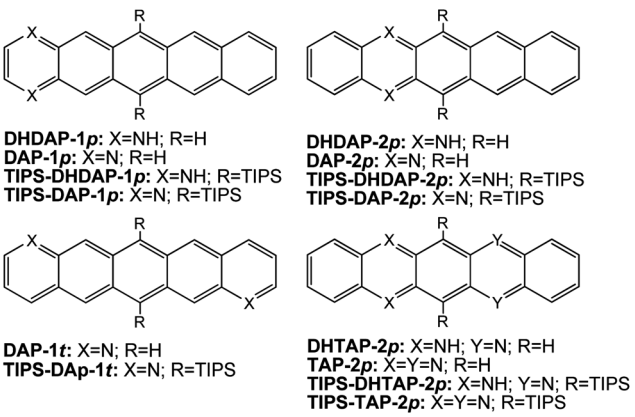

Fig. 1 Molecular structures of the systems investigated.

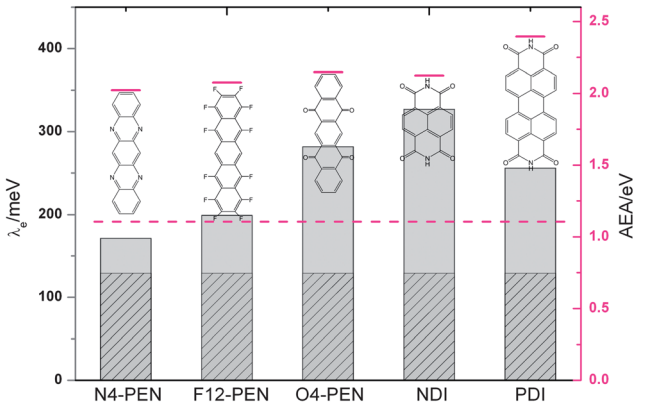

Scheme 1 The electron reorganization (λ_e) and adiabatic electron affinity (AEA) calculated at B3LYP/6-31G* level. (The pink line and the gray bar represent the λ_e and AEA values, respectively. The pink dashed line and the height of the shadow indicate the value of λ_e and AEA for **PEN**, respectively.)

Meanwhile, the introduction of silylethynyl groups to **N-PENs** favors a close two-dimensional (2D) brickwork arrangement in the solid state, such as **TIPS-DHDAP-2*p***, **TIPS-DAP-2*p***, and **TIPS-TAP-2*p*** *etc.*, on the condition that the substitution matches roughly half the width of **N-PENs**. An exception to this rule which was detected is the one-dimensional (1D) π-stacking of **TIPS-DHTAP-2*p*** which has both forms of imine N, that is, NH and N, in the **PEN** architecture. Is there any relationship between the packing arrangement and the number or type of nitrogen atoms in these **N-PENs** derivatives?

The primary aim of our investigation is therefore to ascertain what effect, if any, the dehydrogenation/hydrogenation of **N-PENs** derivatives would have on their electronic structures, packing motifs, and transport properties. To address these issues, theoretical studies on a series of triisopropylsilylethynyl substituted *N*-heteropentacenes (**TIPS-N-PENs**) depicted in Fig. 1 are carried out. We systematically analyze how the variation in the electron–vibration coupling at the single molecular level and the coupling integral estimated from the solid-sate arrangement as a function of the nature and number of nitrogen atoms affects the charge transport of **TIPS-N-PENs**. Considering the limited contribution of silylethynyl to the frontier molecular orbitals (FMOs) and thus the carrier transfer, we take **N-PENs** as the reference systems for their silylethynyl substituted counterparts (**TIPS-N-PENs**) to further estimate whether the properties of **TIPS-N-PENs** could be qualitatively predicted, to some extent, from the relative "smaller size" **N-PENs**. The results clearly demonstrate that the electron transport of the **N-PEN** derivatives can be simply modulated by the removal of hydrogen atoms bonded to nitrogen atoms.

Theoretical methodology

To describe the charge-transport properties of the systems, the incoherent hopping model was employed, in which charge can transfer only between neighboring molecules. Each hopping step has been considered as a nonadiabatic electron-transfer reaction involving the self-exchange charge from a charged molecule to an adjacent neutral one. The rate of charge transfer between

neighboring molecules, k, can be expressed by the standard Marcus equation[43,44] in terms of the reorganization energy λ, the transfer integral V, and the temperature T as:

$$k = \frac{4\pi^2}{h}\frac{1}{\sqrt{4\pi\lambda k_B T}}V^2 \exp\left(-\frac{\lambda}{4k_B T}\right) \quad (1)$$

where h and k_B are the Planck and Boltzmann constants. For a fixed temperature, the large transfer rate can be attributed to the maximal transfer integral and the minimal reorganization energy.

The transfer integral V characterizes the strength of the electronic coupling between two adjacent molecules. It could be obtained from the site-energy corrected method:[45]

$$V_{mn} = \frac{V^0_{mn} - \frac{1}{2}(e_m + e_n)S_{mn}}{1 - S^2_{mn}} \quad (2)$$

Here, $e_{m(n)} = \langle \Phi_{m(n)}|H|\Phi_{m(n)}\rangle$, $V^0_{mn} = \langle \Phi_m|H|\Phi_n\rangle$, and $S_{mn} = \langle \Phi_m|S|\Phi_n\rangle$, where $\Phi_{m(n)}$ is the frontier molecular orbital of the isolated molecule m(n) in the dimer representation. Namely, for hole transport, the highest occupied molecular orbital (HOMO) should be plugged in. H and S are the dimer Hamiltonian and the overlap matrices, respectively.

The reorganization energy λ consists of contributions from the inner reorganization energy λ_i and the external polarization λ_o.[46–48] When the contributions due to the polarization of the medium and to molecular vibrations are neglected,[49,50] the inner reorganization energy is dominant and can be evaluated either from the adiabatic potential-energy surfaces[51,52] or from the normal-mode (NM) analysis.[53–55] The latter approach provides a useful way to understand how the reorganization energy is distributed into the normal modes:

$$\lambda = \sum\lambda_i = \sum\hbar\omega_i S_i, \quad (3)$$

$$\lambda_i = \frac{k_i}{2}\Delta Q_i^2 \quad (4)$$

Here, ΔQ_i represents the displacement along normal mode (NM) i between the equilibrium geometries of the neutral and charged molecules, k_i and ω_i are the corresponding force constants and vibrational frequencies, and S_i denotes the Huang–Rhys factor measuring charge–phonon coupling strength.

To get better insight into the effect of chemical modification on the reorganization process associated with carrier transport, the normal-mode coordinates are expressed by linear combinations of internal coordinates, and the total reorganization energy can thus be projected onto the structural parameters (bond lengths, bond angles, and dihedral angles).[56]

The drift mobility of hopping, μ, can be evaluated from the Einstein relation:

$$\mu = \frac{e}{k_B T}D = \frac{e}{k_B T}\lim_{t\to\infty}\frac{1}{2n}\frac{\langle l(t)^2\rangle}{t} \quad (5)$$

where e is the electronic charge, n is the spatial dimensionality, and l is the hopping distance; D is the diffusion coefficient, simulated by random walk[57,58] here. One molecule is arbitrarily chosen as the starting point, and the charge is only allowed to hop to the nearest neighbor molecules with a probability $P_i = k_i/\sum_i k_i$, where i is the hopping path. At each step, a random number r is uniformly generated between 0 and 1. If $\sum_i^{j-1} P_i < r \le \sum_i^j P_i$, the charge then goes to the neighbor in the jth direction as the next position of the charge. Large numbers of simulations (2000) are performed with each simulation time of 10 μs to get a converged diffusion constant. Normally, 2000 simulations can achieve an error within 5% which is already too small to influence the numerical conclusions.[58,59]

As a comparison, the band model is also employed. In the standard band-theory model, the group velocity $v(k)$ of the delocalized electron waves or hole waves is given by the gradient of the band energy in k-space,

$$\vec{v}(k) = \nabla_k E(k)/\hbar \quad (6)$$

where $E(k)$ is the band energy of the system, k is the wave vector, and $\hbar = h/2\pi$, where h is the Planck constant. In this equation, the charge velocity is proportional to the slope of $E(k)$, that is, the larger the band dispersion is, the higher the mobility is.

Computational details

The equilibrium structures of the neutral and ionic states of 14 **N-PENS** derivatives were fully optimized with the B3LYP functional[60–62] and the 6-31G* basis set[63,64] using the Gaussian 09 program package.[65] A more flexible basis set augmented with additional diffuse and polarization functions (6-31 + G**)[64,66] was also considered, which was proven by our previous study[67] to be important for anionic species. On the basis of the optimized geometries, the harmonic vibrational frequencies were determined by the analytical evaluation of the second derivative of the energy with respect to nuclear displacement. The reorganization energy was evaluated from the relevant points on the potential energy surfaces (adiabatic potential-energy surfaces method), as well as from the normal mode frequencies and vibronic coupling constant in terms of internal coordinates within the framework of Koopmans' theorem approximation, according to the procedure described in detail elsewhere (modified NM analysis).[56] The calculation of charge transfer integrals was performed with the site-energy corrected method at PW91PW91/6-31G* level,[68] and the drift mobility was calculated based on the Marcus equation.[43,44]

Meanwhile, to investigate the main directions of electron transport, the electronic band-structure calculations were performed with VASP[69–71] using the PBE (Perdew–Burke–Ernzerhof) exchange-correlation functional[72] with a plane-wave basis set, and integrations over the Brillouin zone were sampled by $4 \times 4 \times 2$, $8 \times 6 \times 5$, $4 \times 4 \times 2$ and $4 \times 4 \times 2$ k-point meshes for the systems **TIPS-DHDAP-2*p***, **TIPS-DHTAP-2*p***, **TIPS-DAP-2*p*** and **TIPS-TAP-2*p***, respectively, using the Monkhorst–Pack scheme.[73]

Results and discussion

Choice of computational methods

Before exploring any correlation of the DFT results with the molecular properties, the basis set and density functional dependence should be examined. The neutral and ionic geometrical structures of four selected systems **TIPS-DHDAP-2*p***, **TIPS-DHTAP-2*p***, **TIPS-DAP-2*p***, and **TIPS-TAP-2*p*** were

optimized with B3LYP functionals at the 6-31G* and 6-31 + G** levels. According to the calculations of the adiabatic potential surfaces, the reorganization energies of the four systems are collected in Table S1.† It can be seen that the polarization functions on the hydrogen atoms and the diffuse functions on the heavy atoms have negligible effects on the values of λ. The economical 6-31G* basis set is good enough for the estimation of the reorganization energy and will be selected for the following discussion.

It was recognized[74–76] that the DFT estimation of the reorganization energy depends largely on the weight of exact Hartree–Fock-like (HF-like) exchange. Four functionals with different HF-like exchange, BLYP (0%), B3LYP (20%), PBE0 (25%), and BHHLYP (50%), were selected for the series of **N-PENs** systems (Fig. S1†). As is clearly visible, similar evolutions of λ with the number and position of imine N for the various density functionals are observed, although both λ_e and the hole reorganization energy (λ_h) of all **N-PENs** increases with the increasing percentage of HF-like exchange. Among the standard functionals used, B3LYP has been shown to provide an accurate description of the relaxation processes for many oligoacenes and oligothiophenes;[20,77–80] as a result, the B3LYP functional with the 6-31G* basis set was chosen here for the calculations of the geometrical and electrical structures of the **N-PENs** derivatives.

Dehydrogenation effect on the FMOs

The ionization potential (IP) or HOMO level and the EA or lowest unoccupied molecular orbital (LUMO) level are important parameters for organic dyes used in electronic devices. A good n-type conducting material is required to have a high EA or low LUMO for reducing the charge injection barrier from the contact cathode. The contour plots and energies of the HOMOs and LUMOs for representative molecules are displayed in Fig. 2 and listed in Table S2.† Since the inclusion of electronic correlations, the Kohn–Sham LUMO energies fail to predict the EA, as indicted in Table S2.† However, both the EA and the negative LUMO levels present a similar evolution as a function of the number and position of nitrogen atoms. Several general trends in Fig. 2 and Table S2† can be observed.

The first important observation is that the LUMO energy levels decrease markedly going from hydrogenated species to their dehydrogenated congeners, while the opposite is true for the HOMO levels in proceeding from the dehydrogenated forms to the reduced ones. As can be seen from Fig. 2, replacing the CH groups with NH fragments ("CH"/NH substitution) in the **PEN** core (**DHDAP-1*p*** and **DHDAP-2*p***) increases both the HOMO and LUMO energy levels by about 0.05–0.32 and 0.86–1.12 eV, respectively. **DHDAP-1*p***, featuring two contrapuntal NH groups at the terminal ring, presents the highest HOMO energy level here, even larger than that of the p-type semiconductor **PEN**. The "CH"/N substitution in the **PEN** framework (**DAP-1*p***, **DAP-1*t***, **DAP-2*p***, and **TAP-2*p***), however, leads to a stabilization of 0.31–1.05 eV for the HOMOs and 0.37–0.97 eV for the LUMOs. The **DHD(T)AP** series has 2 more electrons than the 22π electrons species, **D(T)AP** and **PEN**. From the hydrogenated 24π electron compounds to the dehydrogenated 22π electron congeners, the LUMO levels are significantly reduced, indicating an evident improvement in the ability for electron injection, resulting from the dehydrogenation process. Inspection of the wavefunctions provides a rationalization for the changes. The LUMOs of **D(T)APs**, resembling that of **PEN**, have a large orbital density over the four longitudinal C–C bonds of both the terminal benzene rings and the nodal points on the center C atoms, as well as between the C–N anti-bonds. Both **PEN** and **D(T)APs** have two Clar six-membered benzenoid rings on either side of the LUMO, while the **DHD(T)APs** only have one terminal Clar ring away from the NH moieties. A general trend exists that the more sextet rings in the orbital, the lower the energy level.[40,81] Therefore, apart from the more electron-deficient nature of N relative to NH or CH segments, the stabilized LUMO levels of the dehydrogenated species benefit to some extent from having two Clar rings instead of one in their corresponding hydrogenated derivatives.

It is worth noting that the evolution of the FMO energy levels of the **TIPS-N-PENs** retains the same trend as their parent **N-PENs** going from the hydrogenated to the dehydrogenated species, since the HOMOs and LUMOs of **TIPS-N-PENs** are very similar in character to those of **N-PENs** except for a few contributions from alkynyl C≡C. As illustrated in Fig. 2, for

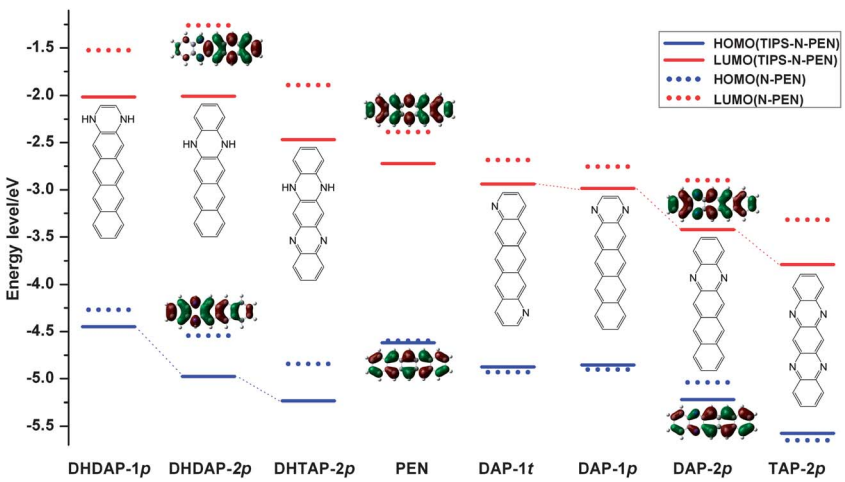

Fig. 2 Relative HOMO and LUMO energy levels of the systems investigated by the B3LYP/6-31G* method.

example, the magnitudes of the stabilization in the HOMO or LUMO from **TIPS-DHDAP-1*p*** to **TIPS-DAP-1*p*** mirror those shown between **DHDAP-1*p*** and **DAP-1*p***, suggesting the dominant effect of **N-PENs** on the FMO energy levels.

Another interesting aspect of these energy diagrams concerns the different sensitivities of the energy levels in the **N-PENs** derivatives to the position of nitrogen atoms; that is, the HOMOs of the hydrogenated species and the LUMOs of the dehydrogenated ones are more sensitive to the location of N than their corresponding LUMOs and HOMOs, respectively. When the two nitrogen atoms move from the terminal ring (**1*p***) to the neighboring ring (**2*p***), the HOMO energy can decrease by 0.53 eV, coupling with the nearly unchanged LUMO level for **TIPS-DHDAPs**; while in **TIPS-DAPs**, the stabilization of the LUMO level (0.44 eV) is larger than for the HOMO level (0.36 eV). The dependence of the energy levels on the position of the nitrogen substitution relies heavily on the distributions of the FMOs in **N-PENs** derivatives (detailed in Table S3†). In the case of the dehydrogenated category, the segments containing N contribute more to the LUMOs (31–52%) than to the HOMOs (18–36%), and the situation becomes severe as the π-deficient ring resides only on one side of the molecule. It is, thus, reasonable that with more contributions from N in the LUMO, the lower the energy level would be. The decrease for the LUMO from **DAP** to **TAP**, in the progressive sequence of **DAP-1*t*** > **DAP-1*p*** > **DAP-2*p*** > **TAP-2*p*** is just proportional to the percentage of N, which increases in the order 7% < 15% < 25% < 36%. **TIPS-TAP-2*p*** containing four nitrogen atoms exhibits the lowest LUMO energy of −3.78 eV among all the systems. As to the **DHDAP** derivatives, we noticed an unsymmetrical distribution in the HOMOs (Table S3†) with more contributions from the first two rings containing NH (**segment 1** 68–85%) than the last two benzenoid rings (**segment 3** 9–18%) and the HOMOs have much larger coefficients at the nitrogen site in comparison to the corresponding LUMOs. The different degree of nitrogen-dependent HOMO and LUMO levels can, hence, be related to the greater contribution of the nitrogen atoms to the HOMOs (31–37%) than to the LUMOs (4–8%) in the hydrogenated species. Such an unbalanced distribution in the FMOs of **TIPS-N-PENs** provides an opportunity to independently adjust the HOMO and LUMO levels at the same time.

By and large, either hydrogenation or dehydrogenation of the **N-PENs** derivatives will lead to significant changes in the distributions and energies of the FMOs, which will further influence their transport properties.

Dehydrogenation effect on the reorganization energy

The reorganization energy term, λ, describing the strength of the local electron–phonon coupling, can be estimated as the sum of the inner and external reorganization energy. Some recent reports have shown that the external part (λ_o) could be quite small and much smaller than the inner part for organic semiconductors, such as **PEN**, the λ_o of which was predicted to be merely 0.002 eV based on a polarizable force field calculation.[50] Therefore, the λ_o of **PEN** derivatives is neglected here and we focus mainly on the intramolecular contributions to the local coupling.

Fig. 3 depicts the inner reorganization energy for hole (electron) transfer, λ_h (λ_e), obtained from the adiabatic potential-energy surfaces (AP) at the B3LYP/6-31G* level. It is clear that upon going from hydrogenated **DHD(T)APs** to the aromatic **D(T)APs**, the λ_h and λ_e decrease from 35–106 meV and 66–265 meV, respectively. The prominent reduction in the reorganization energies for the aromatic **D(T)APs** can be partially ascribed to the larger delocalization degree of the FMOs compared to those of the formally antiaromatic **DHD(T)APs**. There is general agreement that the delocalization of the extra charge carrier over more aromatic fragments can facilitate the drop in reorganization energies. As stated above, both "CH"/NH and "CH"/N substitution on the **PEN** framework can break its high symmetry and decrease the delocalized nature of the FMOs in **PEN** from which an electron is added or removed. The localized characteristics are more larger in the FMOs for **DHD(T)APs** than for **D(T)APs**. It is thus reasonable to detect smaller geometrical relaxations and reorganization energies in **D(T)APs** than in **DHD(T)APs** on going from neutral to ionic states.

Since the only discrepancy between the hydrogenated and dehydrogenated species is the different bonding nature of the nitrogen atoms, an essential source of the smaller λ, especially for the λ_e, in the **D(T)APs** than in the **DHD(T)APs** may be connected with the local bonding characters concerning the nitrogen atoms which include lone pairs (LP), bonding, antibonding, and nonbonding in the FMOs. The natural bond orbital (NBO) method is employed to analysis the local bonding characters of N in the HOMOs and LUMOs for the hydrogenated **DHDAP-1*p*** and the aromatic **DAP-1*p***, and **DCP-2*p*** (displayed in Fig. 4). The nitrogen centers of **DHDAP-1*p*** feature some sp^3 character suggested by the slight bending of the NH bonds away from the molecular plane. This hydrogenated molecule is a 24π species and the lone pair electrons of the nitrogen atoms lie in the molecular plane and could, therefore, participate in the π electron systems of the molecular backbone. As illustrated in the FMOs of **DHDAP-1*p***, the contribution of the LP_N to the HOMO and LUMO is 39% and 6%, respectively. When the **DHDAP-1*p*** is dehydrogenated, increasing sp^2 characters in

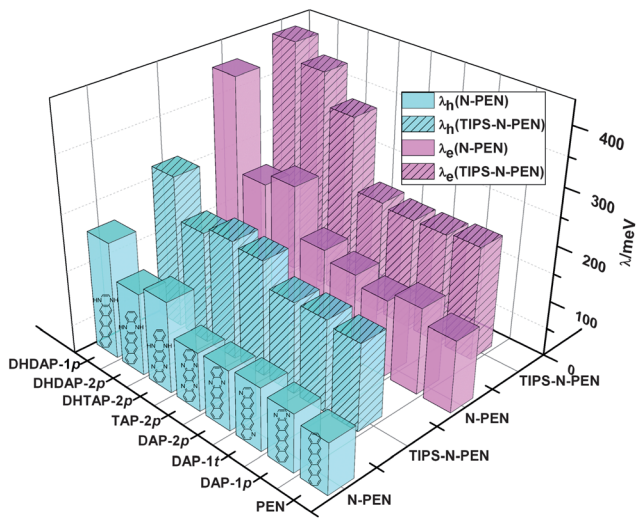

Fig. 3 The reorganization energies evaluated from the adiabatic potential-energy surface.

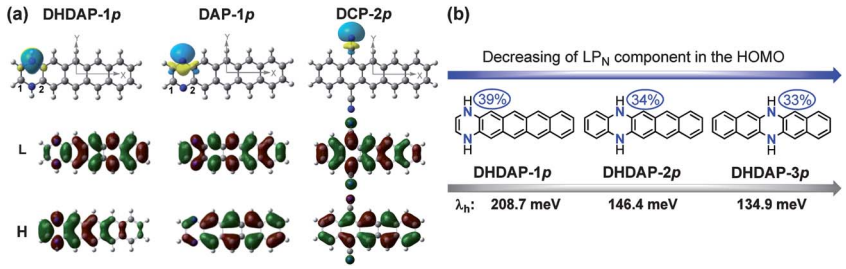

Fig. 4 (a) The frontier molecular orbitals and nitrogen NBO lone pair (LP_N) assignments of **DHDAP-1*p***, **DAP-1*p*** and **DCP-2*p***. (b) The LP_N components of the HOMOs of **DHDAP-1*p***, **DHDAP-2*p*** and **DHDAP-3*p***.

the nitrogen atoms are acquired in **DAP-1*p***, which is an aromatic 22π species just like **PEN**, but has two hydrogen atoms absent at the N sites. The lone pair electrons of the nitrogen atom in **DAP-1*p*** are not part of the aromatic system and extend outwards (along the *y*-axis), different from the delocalized LP_N in **DHDAP-1*p***. The FMOs of **DAP-1*p*** contain π(CN) characters (5%) in the HOMO and 27% π*(CN) in the LUMO. Adding a carrier has more pronounced effects on **DHDAP-1*p*** than on **DAP-1*p*** because a larger contribution to the geometrical relaxation is expected from the delocalized LP_N than from the bonding/antibonding CN. The variations of the C–N distances (ΔCN) from the neutral to ionic molecules are consistent with this picture. Taking hole transport as an example, the absolute values of ΔC_1N and ΔC_2N for the **DHDAP-1*p*** are 0.020 and 0.016 Å, respectively, larger than those for **DAP-1*p***, *i.e.*, 0.006 and 0.011 Å, respectively. Previous studies show that cyano substitution has little effect on the reorganization energy.[78] The same is true in **DCP-2*p***, which has the smallest λ among all the *N*-PENs studied here. The contributions of the bonding π(CN) components to the FMOs of **DCP-2*p*** are of the same order as those of the antibonding π*(CN) part. The resultant nonbonding characters of the cyano groups in the FMOs (shown in Fig. 4) induce a ΔCN no more than 0.001 Å during charge transfer and thus the minimum λ for **DCP-2*p***. Therefore, the donation of the nitrogen part to the reorganization energy roughly follows the order: delocalized LP_N > bonding or antibonding N > nonbonding N.

Since the delocalized LP_N is predicted to closely relate to the large λ values for the hydrogenated **DHDAP** systems, it is natural to expected that the reorganization energies of the **DHDAPs** could be readily tuned by changing the LP_N components in the FMOs. A feasible strategy for this purpose is to alter the position of the nitrogen atoms in the **DHDAPs** from end rings (**DHDAP-1*p***) to center rings (**DHDAP-3*p***). It is clear in Fig. 4b that the λ_h values reduced markedly with the decreasing LP_N components in the HOMOs going from **DHDAP-1*p*** to **DHDAP-2*p*** to **DHDAP-3*p***. The reorganization energies of the hydrogenated **DHDAPs** are found to be sensitive to the location of –NH substitutions. However, the λ values of the dehydrogenated **DAPs** are almost unaffected by the position of the nitrogen atoms. Given that it is the π(CN)/π*(CN) instead of LP_N involved in the FMOs of **DAPs**, we might tentatively infer that the CN contribution to the reorganization energy associated with the charge transfer is limited in the **DAPs**.

In the **TIPS-N-PENs**, the variations of the reorganization energy going from the hydrogenated species to the dehydrogenated ones parallel those for the **N-PENs**, though the values of λ are larger for the **TIPS-N-PENs** than for the **N-PENs** because of the additional contribution from the TIPS moiety as a charge carrier passing through the molecule. In **TIPS-DHDAP**, for example, dehydrogenation on the NH site evidently decreases the λ_e and λ_h by 219 and 117 meV, respectively, and the corresponding values are quite similar for **DHDAP**, *i.e.*, 248 and 106 meV. It is of great interest to question if we can qualitatively evaluate the relative reorganization energy for different **TIPS-N-PENs** by making reference to their corresponding **N-PENs**. To address this issue, the reorganization energies for hole transfer are decomposed into the contributions of each vibrational mode and further projected onto the internal coordinates for **DHDAP-2*p***, **DAP-2*p***, and their derivatives with alkyne substituents, **TIPS-DHDAP-2*p*** and **TIPS-DAP-2*p*** (shown in Fig. 5). It is found that the contributions to the reorganization energy associated with the formation of a positive polaron for **TIPS-DHDAP-2*p*** and **TIPS-DAP-2*p*** mainly come from their parent aromatic parts, **DHDAP-2*p*** and **DAP-2*p***, respectively; while the TIPS components are small, only 36%, in both cases. More precisely, most of the λ_h originates from the relaxation of bond lengths at the same position for both **TIPS-(DH)DAP-2*p*** and **(DH)DAP-2*p***. The predicted contribution of the bond lengths in **TIPS-DHDAP-2*p*** follows the order $C–N_3$ (15.92%) > $C_1–C_1$ (6.26%), consistent with the observations in **DHDAP-2*p***, $C–N_3$ (24.79%) > $C_1–C_1$ (11.12%). As far as **TIPS-DAP-2*p*** and **DAP-2*p*** are concerned, the largest contribution is from the bond length $C_7–C_8$ (12.48% and 15.07%) coupled with 8.25% and 2.87% from $N–C_4$.

Dehydrogenation effect on the intermolecular electronic coupling

Charge transport in organic semiconductors is highly sensitive to the relative orientations of the adjacent molecules and the distribution of their FMOs.[82–85] Therefore, the intermolecular charge transfer integrals (*V*) of the **TIPS-N-PEN** systems studied here are analyzed in terms of the molecular packing and the shape of the FMOs to reach a deeper understanding of the influence of nitrogen centers on the nature of the charge transfer. Starting from the crystal structures reported,[18,19,86] we selected the nearest-neighbor pairs of **TIPS-N-PENs** (shown in Fig. 6 and Fig. S2†) and calculated the *V* value based on the site-energy corrected method using the PW91PW91 functional. Since the sign of *V* arising from the phase of the orbitals has no impact on the evaluation of the charge mobility,[87] the magnitude of *V* is only shown as absolute values.

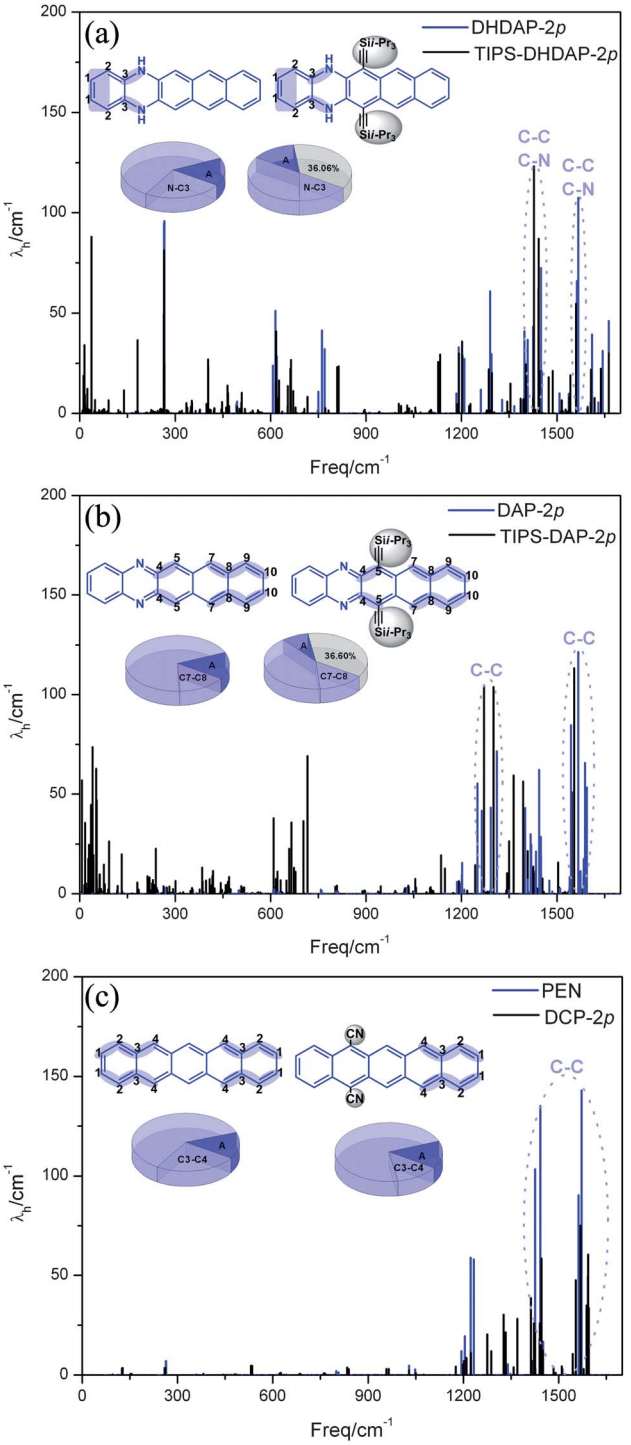

Fig. 5 Contribution of the normal modes and the internal coordinates to the hole reorganization energy for (a) **DHDAP-2*p*** and **TIPS-DHDAP-2*p***; (b) **DAP-2*p*** and **TIPS-DAP-2*p***; (c) **PEN** and **DCP-2*p***. The blue and gray parts in the pie graph represent contributions from the **N-PENs** and TIPS groups, respectively. The bond lengths with a larger contribution to the hole reorganization energy are marked with a blue shadow.

Oligoacenes usually crystallize into herringbone packing arrangements in the solid state, which is not optimal for intermolecular π-orbital overlap. Functionalization of **PEN** with rigid alkynyl spacers can facilitate π-stacking with a favorable two-dimensional brickwork arrangement.[88] As in the case of this work, either hydrogenated **TIPS-DHDAP-2*p*** or dehydrogenated species, **TIPS-DAP-1*p***, **TIPS-DAP-1*t***, **TIPS-DAP-2*p***, and **TIPS-TAP-2*p***, adopt 2D-stacking with two types of close π-packing dimers, D1 and D2, in their crystalline structures. While system **TIPS-DHTAP-2*p*** having hydrogenated and dehydrogenated nitrogen atoms simultaneously in the molecular backbone is arranged with 1D-stacking with only one type of π-dimer, D1. It is interesting to note that the relative orientation of the two molecules within the dimers D1 or D2 for all systems is nearly the same, not only in the π···π distance but also in the relative shifts along the molecular axes. The primary difference between dimer D1 and D2 lies in the spatial overlap between the **PEN** backbones along the molecular long axis, *i.e.*, two benzenoid rings superpositioned in the former and only one in the latter. As a consequence of the larger intermolecular overlap in dimer D1 than in D2 for each system, relatively high electronic couplings could be expected in D1. In most instances, the largest transfer integrals for either holes (V_h) or electrons (V_e) are really observed in D1 with the second largest ones in D2.

It is noticed that the electron couplings of D1 for hydrogenated and dehydrogenated **TIPS-N-PENs** differ much from each other, despite their quite similar intermolecular orientations. A general trend is observed that, from the hydrogenated to the dehydrogenated species, the hole transfer integrals of D1 decreased dramatically, while the opposite trend is found for the electron transfer integrals. As shown in Fig. 6, the V_e of D1 increases in the order: **TIPS-DHDAP-2*p*** (20.8 meV) < **TIPS-DHTAP-2*p*** (21.5 meV) < **TIPS-DAP-2*p*** (99 meV) < **TIPS-TAP-2*p*** (101 meV), and the decrease of V_h follows **TIPS-DHDAP-2*p*** (68.5 meV) > **TIPS-DHTAP-2*p*** (23.0 meV) > **TIPS-DAP-2*p*** (2.9 meV) > **TIPS-TAP-2*p*** (0.06 meV). A similar variation of the transfer integrals is also observed in D2. For example, the V_h (V_e) of **TIPS-DHDAP-2*p*** in D2 is 41.3 meV (34.1 meV), much larger (smaller) than that of the corresponding dehydrogenated **TIPS-DAP-2*p*** (V_h = 1.6 meV, V_e = 46.2 meV). These results indicate that merely concentrating on the spatial superposition without consideration of the distribution of the FMOs cannot lead to an accurate estimation of the electronic coupling. Both the increase of the V_e and the decrease of the V_h in the π-stacking dimers D1 and D2 going from the hydrogenated species to the dehydrogenated ones can be connected with the characteristics of the FMOs mentioned above, that is to say, either "CH"/N or "CH"/NH substitution in the **PEN** framework will break the balanced distribution of FMOs. For the dehydrogenated species, terminal rings containing N involved in the intermolecular overlap contribute more to the LUMO than to the HOMO, and the reverse is true for the hydrogenated congeners. Therefore, the drop in the V_h of D1 from **TIPS-DHDAP-2*p*** to **TIPS-TAP-2*p*** can be simply related to the HOMO orbital overlap between adjacent conjugated molecules, which decreases in the order 42.5% < 40.5% < 30.1% < 21.5% (shown in Fig. 6c); and the increase in the V_e of D1 from **TIPS-DHDAP-2*p*** to **TIPS-TAP-2*p*** is, to some extent, proportional to the improved percentage of the LUMO orbital overlap of the π dimer. Furthermore, the patterns of the FMOs in the dehydrogenated species also facilitate more effective coupling between the LUMOs than the HOMOs, because the nodal planes basically lie parallel to the short axis for the LUMOs, but parallel to both the long and short axes for the HOMOs.[89]

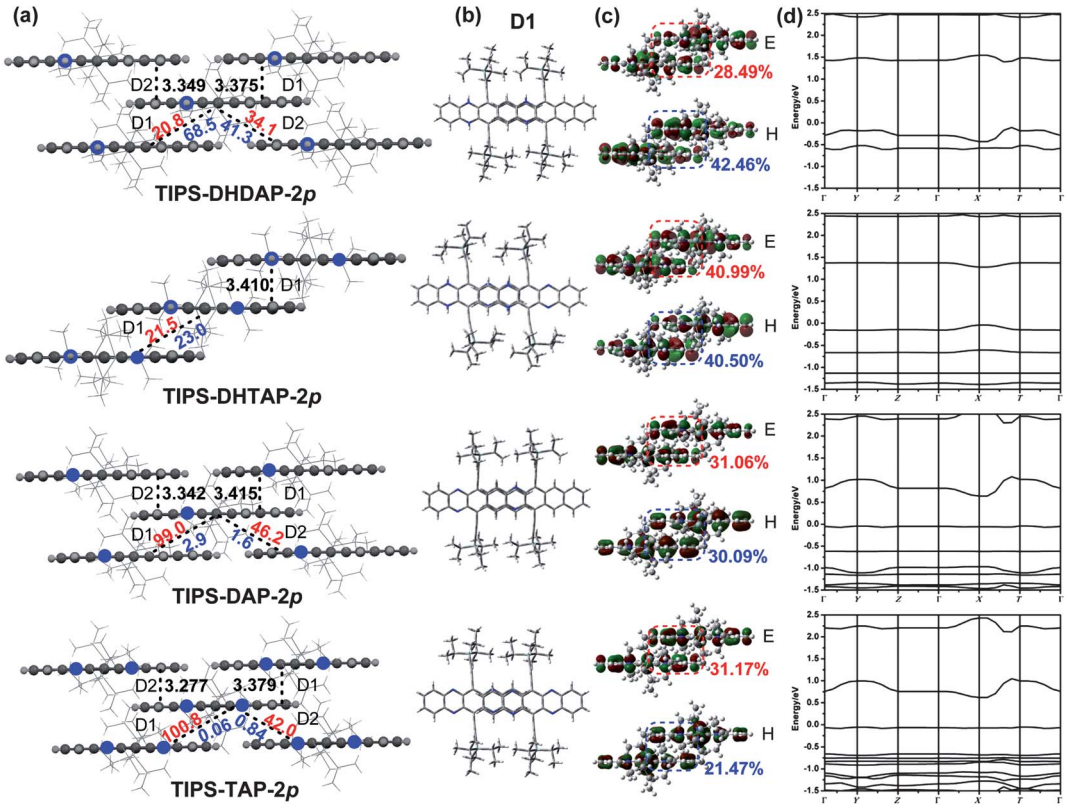

Fig. 6 The main carrier transport pathways and band structures of the systems **TIPS-DHDAP-2*p***, **TIPS-DHTAP-2*p***, **TIPS-DAP-2*p*** and **TIPS-TAP-2*p***. (a) The molecular packings and dimer type pathways (D*n*), the black, red and blue data represent π···π distance, V_e, and V_h of D*n*, respectively. (b) Top view of D1. (c) Side view of the orbital overlap in D1. The overlap proportions of D1, relative to electron and hole transport, are shown in red and blue, respectively. (d) Band structures of four crystals. System **TIPS-DHDAP-2*p***: triclinic space group *P*1, $a = 7.67$ Å, $b = 7.23$ Å, $c = 16.92$ Å, and $\alpha = 78.04°$, $\beta = 88.79°$, $\gamma = 81.66°$; System **TIPS-DHTAP-2*p***: triclinic space group *P*1, $a = 8.06$ Å, $b = 10.51$ Å, $c = 12.76$ Å, and $\alpha = 99.83°$, $\beta = 100.78°$, $\gamma = 101.53°$; System **TIPS-DAP-2*p***: triclinic space group *P*1, $a = 7.66$ Å, $b = 7.72$ Å, $c = 16.98$ Å, and $\alpha = 78.23°$, $\beta = 88.76°$, $\gamma = 81.78°$; System **TIPS-TAP-2*p***: triclinic space group $P\bar{1}$, $a = 7.58$ Å, $b = 7.61$ Å, $c = 16.84$ Å, and $\alpha = 78.98°$, $\beta = 89.54°$, $\gamma = 81.90°$.The energies are plotted along the directions in the first Brillouin zone connecting the points: $\Gamma = (0, 0, 0)$, $Y = (0, 0.5, 0)$, $Z = (0, 0, 0.5)$, $X = (0.5, 0, 0)$, $T = (0, 0.5, 0.5)$, for the band structures of all systems. The zero of the energy scale is set as the Fermi level.

Based on the evaluation of λ and V, the drift mobilities of holes and electrons, *i.e.*, μ_h and μ_e, were estimated at 300 K from eqn (1) and (5) for all **TIPS-N-PENs** studied here. The calculated results are listed in Table 1 with the available experimental data. It is clear from the experimental and theoretical results that the electron mobilities of **TIPS-N-PENs** are largely improved upon dehydrogenation. The measured electron mobility for dehydrogenated **TIPS-TAP-2*p*** is up to 3.3 $cm^2\ V^{-1}\ s^{-1}$, while devices fabricated from hydrogenated **TIPS-N-PENs** don't show any n-type behavior. The electron mobility of the dehydrogenated species is predicted to increase by about 1 to 3 orders of magnitude over the hydrogenated ones.

In order to further understand the anisotropic charge transport in crystals, the band structures of the systems **TIPS-DHDAP-2*p***, **TIPS-DHTAP-2*p***, **TIPS-DAP-2*p*** and **TIPS-TAP-2*p*** (Fig. 6d) were also examined. The conduction and valence bands of the four systems do not possess degenerate character due to the presence of only one molecule in their primitive unit cells. The paths with a big transfer integral are all along the directions with large dispersions in the valence band (VB) and conduction band (CB). As shown in Fig. 6d, for **TIPS-DHTAP-2*p***, the strongest VB and CB dispersions both occur in the ΓX subzone, corresponding to the *a*-axis (D1 direction) in real space, and the biggest dispersions in the VB and CB are almost the same, suggesting its ambipolar transport potential. As to the systems **TIPS-DHDAP-2*p***, **TIPS-DAP-2*p***, and **TIPS-TAP-2*p***, their largest VBs and CBs disperse asymmetrically in the XT sections, *i.e.*, the *ab*-plane in real space, indicating the possibility of 2D charge transfer for either holes or electrons. Hole transport is preferred in the system **TIPS-DHDAP-2*p***, because the biggest

Table 1 The calculated[a] and experimental[b] mobility ($cm^2\ V^{-1}\ s^{-1}$) of the systems investigated

system	μ_e[a]	μ_h[a]	μ_e[b]	μ_h[b]
TIPS-DHDAP-2*p*	1.149×10^{-1}	3.119×10^{0}		0.02–0.07
TIPS-DHTAP-2*p*	4.480×10^{-2}	2.162×10^{-1}		
TIPS-DAP-1*p*	7.145×10^{0}	3.446×10^{-1}		0.3–1.2
TIPS-DAP-1*t*	7.441×10^{0}	5.766×10^{-1}	0.15	0.11
TIPS-DAP-2*p*	5.565×10^{0}	1.153×10^{-2}	$2–4 \times 10^{-4}$	0.02–0.05
TIPS-TAP-2*p*	4.994×10^{0}	6.652×10^{-3}	1.0–3.3	

[a] The average mobility calculated with the diffusion constant *D* simulated by random walk. [b] Experimental values from ref. 18, 19 and 86.

dispersion in the CB is smaller than that in the VB. However, in the systems **TIPS-DAP-2*p*** and **TIPS-TAP-2*p***, the strongly dispersive CB and the flat VBs in all directions suggest their capability for electron transport. Importantly, upon dehydrogenation of **TIPS-N-PENs**, similar variations in the charge transfer from holes to electrons is also predicted from their electronic band structures.

Comparing the crystal structures of these **TIPS-N-PENs** systems, an interesting phenomenon attracting our attention is that only **TIPS-DHTAP-2*p*** (having both N and NH centers in the molecular architecture) presents 1D π-stacking, while the others (containing either N or NH segments) favor a close 2D brickwork arrangement. Since the charge transfer is closely related to the packing motif, it is particularly important here to ascertain what effect, if any, the type of nitrogen centers would have on the stacking of **TIPS-N-PEN**. In this sense, the 1D-parallel **TIPS-DHTAP-2*p*** was artificially transformed into a 2D-brick arrangement to understand the driving forces of the aromatic stacking interactions in the 1D **TIPS-DHTAP-2*p***. Two classical intermolecular orientations are inset in Fig. 7. The first one is a 1D-parallel cluster involving 5 molecules selected from the crystal structures of **TIPS-DHTAP-2*p***. The second one is the 2D-brick cluster, which is built from a 1D-parallel cluster with three molecules fixed (shown in grey wireframe) and the remaining two molecules (shown in black tube) displaced along the longitudinal axis by an amount *r*. The unrelaxed potential energy surface (UPES) of **TIPS-DHTAP-2*p*** as a function of *r* is calculated using the dispersion-corrected ωB97XD, B97D, or B3LYP-D exchange-correlation functionals and the 3-21G* basis set (shown in Fig S3†). These three functionals including the empirical dispersion which have been reported to treat van der Waals interactions more accurately than other functionals.[90–93] It is clear that the three methods show quite similar energy-evolution trends, and the molecular cluster of **TIPS-DHTAP-2*p*** prefers 1D-parallel over 2D-brick arrangements. However, we cannot know if the relatively stable 1D packing comes from the π···π or CH···π interactions. To assess the role of π···π interactions in the 1D motif, we also evaluate the UPES of **DHTAP-2*p*** at the same levels with cluster models referencing those of **TIPS-DHTAP-2*p***. The three methods all indicate that a 2D-brick motif in **DHTAP-2*p*** is more stable than the 1D arrangement. Comparing the results of **TIPS-DHTAP-2*p*** and **DHTAP-2*p***, we may tentatively ascribe the 1D-parallel structure in **TIPS-DHTAP-2*p*** to vigorous CH···π interactions since much stronger π···π interactions are obtained in the 2D packing than in the 1D arrangement.

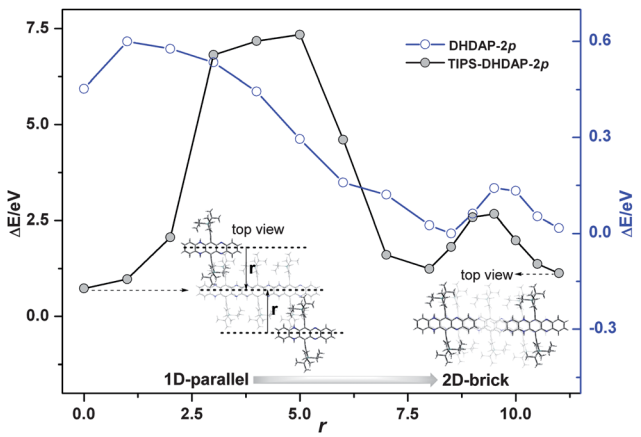

Fig. 7 The relative energy curves of **DHTAP-2*p*** (blue) and **TIPS-DHTAP-2*p*** (black) from 1D-parallel to 2D-brick arrangement at ωB97XD/3-21G* level.

Based on the unrelaxed geometry, the UPES only provides a rough estimation of the driving force of 1D-packing of **TIPS-DHTAP-2*p***. To verify our assumption, two cluster models of **TIPS-DHTAP-2*p*** with 1D- and 2D-packing were fully optimized with the ωB97XD/3-21G* method, and the BSSE-corrected bonding energies (Fig. 8b) between three fixed molecules and two moved molecules were evaluated at the same level. The results of the calculation lead to an estimated binding energy of −40.3 kcal mol^{-1} for the 1D-parallel arrangement, larger than that for the 2D-brick model by 14 kcal mol^{-1}. This points again to the C–H···π interaction dependent 1D-packing in the system **TIPS-DHTAP-2*p***.

The intense C–H···π interactions in **TIPS-DHTAP-2*p*** can be connected with the type of substituted nitrogen atoms. As illustrated in Fig. 8a, the "CH"/N or "CH"/NH substitution in the **PEN** framework will change the electron density distribution of **PEN**. In the system **DHDAP-2*p***, the location of the rings containing NH groups is electron-deficient, while for **TAP-2*p***, the ring containing N centers is electron-rich. When both "CH"/N and "CH"/NH substitutions simultaneously exist in the **PEN** architecture, as in the case of **DHTAP-2*p***, increased intramolecular charge transfer will accumulate more negative charge at the N sites. Thus, for the **TIPS-DHTAP-2*p*** crystal, strong C–H···π interactions can be obtained *via* electrostatic attraction between the positive TIPS group and the negative CN edges. This dominating C–H···π interaction in the 1D-stacking architecture is illustrated in Fig. S4† from NBO analysis and identified by

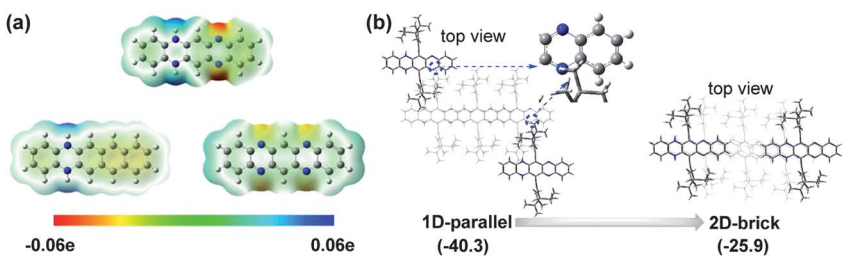

Fig. 8 (a) The electrostatic potential maps of **DHDAP-2*p***, **DHTAP-2*p***, and **TAP-2*p*** calculated by the B3LYP/6-31G* method. (b) The BSSE-corrected bonding energy of **TIPS-DHTAP-2*p*** in 1D-parallel and 2D-brick arrangement calculated at ωB97XD/3-21G* level.

looking at the shortest intermolecular contacts presented in the **TIPS-DHTAP-2*p*** crystal structure.

Conclusion

For the design of electron transfer materials, a low LUMO level (high electron affinity), a small molecular reorganization energy and large intermolecular charge transfer integrals are necessary. In this work, we demonstrate that the dehydrogenation of **N-PENs** derivatives presents an integrated three-in-one advantage for transforming p-type semiconductors to n-type. First, the dehydrogenation of **N-PENs** lowers the LUMO levels by at least 1 eV, which can facilitate electron injection. We found that for such systems, the LUMO level is more sensitive to the location of N than the HOMO since the segments containing N contribute more to the LUMO than to the HOMO. This provides an opportunity to adjust the LUMO level, independent of the HOMO level. Secondly, the dehydrogenated systems have smaller charge reorganization energies than their hydrogenated congeners, which is attributed to the different bonding nature of the nitrogen atoms, as analyzed from modified normal mode analysis and NBO. The contribution of the nitrogen segments to the reorganization energy follows the order: delocalized LP_N (existing in hydrogenated systems) > bonding or antibonding N (existing in dehydrogenated systems) > nonbonding N (existing in cyanated systems). The reorganization energies of the hydrogenated **N-PENs** are found to be sensitive to the location of –NH substitutions, while the values of λ for dehydrogenated **N-PENs** are almost unaffected by the position of nitrogen atoms.

Lastly, from the hydrogenated to the dehydrogenated species, the electron transfer integrals of π-dimers increase dramatically. The relatively large electron transfer integrals in the latter come from the increased LUMO overlap of the π dimer. The calculations also reveal that when both types of imine N, (NH and N) coexist in the molecular backbone, the **TIPS-N-PENs** favor a 1D π-stacking over a close 2D brickwork arrangement as a result of the improved intermolecular C–H$\cdots\pi$ interactions. Band structure calculations also predict larger dispersion in the VB than in the CB for the dehydrogenated **TIPS-N-PENs**, which is consistent with the dimer calculations. In conclusion, our theoretical study provides deeper insight into the relationship between single molecular structure and the charge transport properties of **N-PENs** derivatives at the molecular level, which is helpful for the design of materials with a large electron mobility prior to chemical synthesis.

Acknowledgements

The authors gratefully acknowledge financial support from the Program for New Century Excellent Talents in University of China (NCET-10-0011), the Scientific Research Common Program of Beijing Municipal Education Commission (No. KM201110028007), the National Natural Science Foundation of China (Grant Nos. 90921007, 20920102031) and the Ministry of Science and Technology through the 973 program (Grant Nos. 2009CB623600, 2011CB932304, 2011CB808405).

References

1 Y. Qiao, J. Zhang, W. Xu and D. Zhu, *J. Mater. Chem.*, 2012, **22**, 5706–5714.
2 Y. Qiao, Y. Guo, C. Yu, F. Zhang, W. Xu, Y. Liu and D. Zhu, *J. Am. Chem. Soc.*, 2012, **134**, 4084–4087.
3 M. Treier, J.-B. Arlin, C. Ruzie, Y. H. Geerts, V. Lemaur, J. Cornil and P. Samori, *J. Mater. Chem.*, 2012, **22**, 9509–9512.
4 H. E. Katz, A. J. Lovinger, J. Johnson, C. Kloc, T. Siegrist, W. Li, Y. Y. Lin and A. Dodabalapur, *Nature*, 2000, **404**, 478–481.
5 Z. Zhao, S. Chen, C. Deng, J. W. Y. Lam, C. Y. K. Chan, P. Lu, Z. Wang, B. Hu, X. Chen, H. S. Kwok, Y. Ma, H. Qiu and B. Z. Tang, *J. Mater. Chem.*, 2011, **21**, 10949–10956.
6 Y.-J. Pu, G. Nakata, F. Satoh, H. Sasabe, D. Yokoyama and J. Kido, *Adv. Mater.*, 2012, **24**, 1765–1770.
7 C.-Z. Li, H.-L. Yip and A. K. Y. Jen, *J. Mater. Chem.*, 2012, **22**, 4161–4177.
8 A. T. Yiu, P. M. Beaujuge, O. P. Lee, C. H. Woo, M. F. Toney and J. M. J. Fréchet, *J. Am. Chem. Soc.*, 2011, **134**, 2180–2185.
9 J. You, M.-F. Lo, W. Liu, T.-W. Ng, S.-L. Lai, P. Wang and C.-S. Lee, *J. Mater. Chem.*, 2012, **22**, 5107–5113.
10 X. Guo, R. P. Ortiz, Y. Zheng, M.-G. Kim, S. Zhang, Y. Hu, G. Lu, A. Facchetti and T. J. Marks, *J. Am. Chem. Soc.*, 2011, **133**, 13685–13697.
11 Y. Chen, H. Tian, Y. Geng, J. Chen, D. Ma, D. Yan and L. Wang, *J. Mater. Chem.*, 2011, **21**, 15332–15336.
12 Y. Li, S. P. Singh and P. Sonar, *Adv. Mater.*, 2010, **22**, 4862–4866.
13 I. Osaka, T. Abe, S. Shinamura, E. Miyazaki and K. Takimiya, *J. Am. Chem. Soc.*, 2010, **132**, 5000–5001.
14 X. L. Feng, V. Marcon, W. Pisula, M. R. Hansen, J. Kirkpatrick, F. Grozema, D. Andrienko, K. Kremer and K. Mullen, *Nat. Mater.*, 2009, **8**, 421–426.
15 I. McCulloch, M. Heeney, C. Bailey, K. Genevicius, I. MacDonald, M. Shkunov, D. Sparrowe, S. Tierney, R. Wagner, W. Zhang, M. L. Chabinyc, R. J. Kline, M. D. McGehee and M. F. Toney, *Nat. Mater.*, 2006, **5**, 328–333.
16 Q. Tang, D. Zhang, S. Wang, N. Ke, J. Xu, J. C. Yu and Q. Miao, *Chem. Mater.*, 2009, **21**, 1400–1405.
17 Z. Liang, Q. Tang, J. Liu, J. Li, F. Yan and Q. Miao, *Chem. Mater.*, 2010, **22**, 6438–6443.
18 Z. Liang, Q. Tang, J. Xu and Q. Miao, *Adv. Mater.*, 2011, **23**, 1535–1539.
19 Z. Liang, Q. Tang, R. Mao, D. Liu, J. Xu and Q. Miao, *Adv. Mater.*, 2011, **23**, 5514–5518.
20 H.-Y. Chen and I. Chao, *ChemPhysChem*, 2006, **7**, 2003–2007.
21 M. Winkler and K. N. Houk, *J. Am. Chem. Soc.*, 2007, **129**, 1805–1815.
22 X.-K. Chen, J.-F. Guo, L.-Y. Zou, A.-M. Ren and J.-X. Fan, *J. Phys. Chem. C*, 2011, **115**, 21416–21428.
23 S. Chai, S.-H. Wen, J.-D. Huang and K.-L. Han, *J. Comput. Chem.*, 2011, **32**, 3218–3225.
24 C.-H. Li, C.-H. Huang and M.-Y. Kuo, *Phys. Chem. Chem. Phys.*, 2011, **13**, 11148–11155.
25 U. H. F. Bunz, *Chem.–Eur. J.*, 2009, **15**, 6780–6789.
26 U. H. F. Bunz, *Pure Appl. Chem.*, 2010, **82**, 953–968.
27 O. Tverskoy, F. Rominger, A. Peters, H.-J. Himmel and U. H. F. Bunz, *Angew. Chem., Int. Ed.*, 2011, **50**, 3557–3560.
28 C.-L. Song, C.-B. Ma, F. Yang, W.-J. Zeng, H.-L. Zhang and X. Gong, *Org. Lett.*, 2011, **13**, 2880–2883.
29 J. U. Engelhart, B. D. Lindner, O. Tverskoy, F. Rominger and U. H. F. Bunz, *Org. Lett.*, 2012, **14**, 1008–1011.
30 Q. Miao, *Synlett*, 2012, **23**, 326–336.
31 J. Fleischhauer, S. Zahn, R. Beckert, U.-W. Grummt, E. Birckner and H. Görls, *Chem.–Eur. J.*, 2012, **18**, 4549–4557.
32 Q. Miao, T.-Q. Nguyen, T. Someya, G. B. Blanchet and C. Nuckolls, *J. Am. Chem. Soc.*, 2003, **125**, 10284–10287.
33 C. Seillan, H. Brisset and O. Siri, *Org. Lett.*, 2008, **10**, 4013–4016.
34 G. J. Richards, J. P. Hill, T. Mori and K. Ariga, *Org. Biomol. Chem.*, 2011, **9**, 5005–5017.
35 Q. Tang, J. Liu, H. S. Chan and Q. Miao, *Chem.–Eur. J.*, 2009, **15**, 3965–3969.
36 R. Scipioni, M. Boero, G. J. Richards, J. P. Hill, T. Ohno, T. Mori and K. Ariga, *J. Chem. Theory Comput.*, 2010, **6**, 517–525.
37 R. Scipioni, J. P. Hill, G. J. Richards, M. Boero, T. Mori, K. Ariga and T. Ohno, *Phys. Chem. Chem. Phys.*, 2011, **13**, 2145–2150.

38 A. L. Appleton, S. M. Brombosz, S. Barlow, J. S. Sears, J.-L. Brédas, S. R. Marder and U. H. F. Bunz, *Nat. Commun.*, 2010, **1**, 91.
39 K. E. Maly, *Cryst. Growth Des.*, 2011, **11**, 5628–5633.
40 J. I. Wu, C. S. Wannere, Y. Mo, P. V. R. Schleyer and U. H. F. Bunz, *J. Org. Chem.*, 2009, **74**, 4343–4349.
41 S.-Z. Weng, P. Shukla, M.-Y. Kuo, Y.-C. Chang, H.-S. Sheu, I. Chao and Y.-T. Tao, *ACS Appl. Mater. Interfaces*, 2009, **1**, 2071–2079.
42 M. M. Islam, S. Pola and Y.-T. Tao, *Chem. Commun.*, 2011, **47**, 6356–6358.
43 R. A. Marcus, *Rev. Mod. Phys.*, 1993, **65**, 599–610.
44 V. Balzani, A. Juris, M. Venturi, S. Campagna and S. Serroni, *Chem. Rev.*, 1996, **96**, 759–833.
45 E. F. Valeev, V. Coropceanu, D. A. da Silva Filho, S. Salman and J.-L. Brédas, *J. Am. Chem. Soc.*, 2006, **128**, 9882–9886.
46 B. S. Brunschwig, J. Logan, M. D. Newton and N. Sutin, *J. Am. Chem. Soc.*, 1980, **102**, 5798–5809.
47 P. Siders and R. A. Marcus, *J. Am. Chem. Soc.*, 1981, **103**, 748–752.
48 M. D. Newton and N. Sutin, *Annu. Rev. Phys. Chem.*, 1984, **35**, 437–480.
49 I. Vilfan, *Phys. Status Solidi B*, 1973, **59**, 351–360.
50 J. E. Norton and J. L. Brédas, *J. Am. Chem. Soc.*, 2008, **130**, 12377–12384.
51 H. Z. Gao, C. S. Qin, H. Y. Zhang, S. X. Wu, Z. M. Su and Y. Wang, *J. Phys. Chem. A*, 2008, **112**, 9097–9103.
52 X. D. Tang, H. Z. Gao, Y. Geng, Y. Liao and Z. M. Su, *Chem. J. Chin. Univ.*, 2010, **31**, 766–771.
53 J. R. Reimers, *J. Chem. Phys.*, 2001, **115**, 9103–9109.
54 Y. Geng, J. P. Wang, S. X. Wu, H. B. Li, F. Yu, G. H. Yang, H. Z. Gao and Z. M. Su, *J. Mater. Chem.*, 2011, **21**, 134–143.
55 Y. Geng, S.-X. Wu, H.-B. Li, X.-D. Tang, Y. Wu, Z.-M. Su and Y. Liao, *J. Mater. Chem.*, 2011, **21**, 15558–15566.
56 H. Geng, Y. Niu, Q. Peng, Z. Shuai, V. Coropceanu and J.-L. Brédas, *J. Chem. Phys.*, 2011, **135**, 104703–104707.
57 G. Nan, L. Wang, X. Yang, Z. Shuai and Y. Zhao, *J. Chem. Phys.*, 2009, **130**, 024704–024708.
58 G. Nan, X. Yang, L. Wang, Z. Shuai and Y. Zhao, *Phys. Rev. B: Condens. Matter Mater. Phys.*, 2009, **79**, 115203.
59 H. Geng, Q. Peng, L. J. Wang, H. J. Li, Y. Liao, Z. Y. Ma and Z. G. Shuai, *Adv. Mater.*, 2012, **24**, 3568–3572.
60 A. D. Becke, *Phys. Rev. A: At., Mol., Opt. Phys.*, 1988, **38**, 3098–3100.
61 C. T. Lee, W. T. Yang and R. G. Parr, *Phys. Rev. B*, 1988, **37**, 785–789.
62 P. J. Stephens, F. J. Devlin, C. F. Chabalowski and M. J. Frisch, *J. Phys. Chem.*, 1994, **98**, 11623–11627.
63 W. J. Hehre, R. Ditchfield and J. A. Pople, *J. Chem. Phys.*, 1972, **56**, 2257–2261.
64 P. C. Hariharan and J. A. Pople, *Theor. Chim. Acta*, 1973, **28**, 213–222.
65 G. W. T. M. J. Frisch, H. B. Schlegel, G. E. Scuseria, M. A. Robb, J. R. Cheeseman, G. Scalmani, V. Barone, B. Mennucci, G. A. Petersson, H. Nakatsuji, M. Caricato, X. Li, H. P. Hratchian, A. F. Izmaylov, J. Bloino, G. Zheng, J. L. Sonnenberg, M. Hada, M. Ehara, K. Toyota, R. Fukuda, J. Hasegawa, M. Ishida, T. Nakajima, Y. Honda, O. Kitao, H. Nakai, T. Vreven, J. A. Montgomery Jr, J. E. Peralta, F. Ogliaro, M. Bearpark, J. J. Heyd, E. Brothers, K. N. Kudin, V. N. Staroverov, R. Kobayashi, J. Normand, K. Raghavachari, A. Rendell, J. C. Burant, S. S. Iyengar, J. Tomasi, M. Cossi, N. Rega, J. M. Millam, M. Klene, J. E. Knox, J. B. Cross, V. Bakken, C. Adamo, J. Jaramillo, R. Gomperts, R. E. Stratmann, O. Yazyev, A. J. Austin, R. Cammi, C. Pomelli, J. W. Ochterski, R. L. Martin, K. Morokuma, V. G. Zakrzewski, G. A. Voth, P. Salvador, J. J. Dannenberg, S. Dapprich, A. D. Daniels, O. Farkas, J. B. Foresman, J. V. Ortiz, J. Cioslowski and D. J. Fox, *Gaussian 09W, Revision A.02*, Gaussian, Inc., Wallingford CT, 2009.
66 M. M. Francl, W. J. Pietro, W. J. Hehre, J. S. Binkley, M. S. Gordon, D. J. DeFrees and J. A. Pople, *J. Chem. Phys.*, 1982, **77**, 3654–3665.
67 X.-D. Tang, Y. Liao, H.-Z. Gao, Y. Geng and Z.-M. Su, *J. Mater. Chem.*, 2012, **22**, 6907–6918.
68 J. Huang and M. Kertesz, *Chem. Phys. Lett.*, 2004, **390**, 110–115.
69 G. Kresse and J. Hafner, *Phys. Rev. B: Condens. Matter*, 1993, **47**, 558–561.
70 G. Kresse and J. Hafner, *Phys. Rev. B: Condens. Matter*, 1994, **49**, 14251–14269.
71 G. Kresse and J. Furthmüller, *Comput. Mater. Sci.*, 1996, **6**, 15–50.
72 J. P. Perdew, K. Burke and M. Ernzerhof, *Phys. Rev. Lett.*, 1996, **77**, 3865–3868.
73 J. D. Pack and H. J. Monkhorst, *Phys. Rev. B: Solid State*, 1977, **16**, 1748.
74 J. C. Sancho-García, *Chem. Phys.*, 2007, **331**, 321–331.
75 J. C. Sancho-Garcia and A. J. Perez-Jimenez, *J. Chem. Phys.*, 2008, **129**, 024103–024114.
76 J. C. Sancho-García and A. J. Pérez-Jiménez, *J. Phys. Chem. A*, 2008, **112**, 10325–10332.
77 S. T. Bromley, M. Mas-Torrent, P. Hadley and C. Rovira, *J. Am. Chem. Soc.*, 2004, **126**, 6544–6545.
78 M.-Y. Kuo, H.-Y. Chen and I. Chao, *Chem.–Eur. J.*, 2007, **13**, 4750–4758.
79 M. C. R. Delgado, K. R. Pigg, D. T. A. da Silva Filho, N. E. Gruhn, Y. Sakamoto, T. Suzuki, R. M. Osuna, J. Casado, V. c. Hernández, J. T. L. p. Navarrete, N. G. Martinelli, J. Cornil, R. S. Sánchez-Carrera, V. Coropceanu and J.-L. Brédas, *J. Am. Chem. Soc.*, 2009, **131**, 1502–1512.
80 E. G. Kim, V. Coropceanu, N. E. Gruhn, R. S. Sanchez-Carrera, R. Snoeberger, A. J. Matzger and J. L. Bredas, *J. Am. Chem. Soc.*, 2007, **129**, 13072–13081.
81 S. Miao, S. M. Brombosz, P. V. R. Schleyer, J. I. Wu, S. Barlow, S. R. Marder, K. I. Hardcastle and U. H. F. Bunz, *J. Am. Chem. Soc.*, 2008, **130**, 7339–7344.
82 J. L. Brédas, J. P. Calbert, D. A. da Silva Filho and J. Cornil, *Proc. Natl. Acad. Sci. U. S. A.*, 2002, **99**, 5804–5809.
83 C. R. Newman, C. D. Frisbie, D. A. da Silva Filho, J.-L. Brédas, P. C. Ewbank and K. R. Mann, *Chem. Mater.*, 2004, **16**, 4436–4451.
84 J. E. Norton and J.-L. Brédas, *J. Chem. Phys.*, 2008, **128**, 034701–034707.
85 Y. Geng, H. Li, S. Wu and Z. Su, *J. Mater. Chem.*, 2012, DOI: 10.1039/c2jm33369d.
86 Y.-Y. Liu, C.-L. Song, W.-J. Zeng, K.-G. Zhou, Z.-F. Shi, C.-B. Ma, F. Yang, H.-L. Zhang and X. Gong, *J. Am. Chem. Soc.*, 2010, **132**, 16349–16351.
87 S. E. Koh, C. Risko, D. A. da Silva Filho, O. Kwon, A. Facchetti, J. L. Brédas, T. J. Marks and M. A. Ratner, *Adv. Funct. Mater.*, 2008, **18**, 332–340.
88 J. E. Anthony, D. L. Eaton and S. R. Parkin, *Org. Lett.*, 2002, **4**, 15–18.
89 A. Troisi, G. Orlandi and J. E. Anthony, *Chem. Mater.*, 2005, **17**, 5024–5031.
90 J.-D. Chai and M. Head-Gordon, *Phys. Chem. Chem. Phys.*, 2008, **10**, 6615–6620.
91 S. Grimme, *J. Comput. Chem.*, 2006, **27**, 1787–1799.
92 Y.-A. Duan, Y. Geng, H.-B. Li, X.-D. Tang, J.-L. Jin and Z.-M. Su, *Org. Electron.*, 2012, **13**, 1213–1222.
93 J. Antony and S. Grimme, *Phys. Chem. Chem. Phys.*, 2006, **8**, 5287–5293.